



# Porous graphitic carbon nitride nanosheets prepared under self-producing atmosphere for highly improved photocatalytic activity



Xueping Song, Qin Yang, Xiaohui Jiang, Mengyun Yin, Limei Zhou\*

*Chemical Synthesis and Pollution Control Key Laboratory of Sichuan Province, China West Normal University, Nanchong 637002, Sichuan, China*

## ARTICLE INFO

### Article history:

Received 18 February 2017

Received in revised form 26 May 2017

Accepted 28 May 2017

Available online 30 May 2017

### Keywords:

Graphitic carbon nitride

Photocatalysis

Layer distortion

Self-producing atmosphere

## ABSTRACT

The reaction atmosphere employed in graphitic carbon nitride ( $g\text{-C}_3\text{N}_4$ ) synthesis can play an important role in modifying the electronic structure and the properties of photoexcited charge carriers and consequently the photocatalytic activity of semiconductor photocatalysts. By controlling the entrance of  $\text{N}_2$  in the preparation of  $g\text{-C}_3\text{N}_4$ , we introduced pyrolysis-generated self-producing atmosphere. Under the homogeneous self-producing atmosphere and without any other additives, we fabricated porous  $g\text{-C}_3\text{N}_4$  with more uncondensed amino groups. These formed pores endow  $g\text{-C}_3\text{N}_4$  nanosheets with more exposed active edges and cross-plane diffusion channels that greatly speed up mass and charge carrier transfer. Furthermore, the uncondensed amino groups within the structure could promote the dispersion behavior of samples in water and induce the structure distortion of  $g\text{-C}_3\text{N}_4$  layers through the strong hydrogen bonding interactions between layers and thus decease the distance of interlayers. Enhanced photocatalytic activity is seen as well from a drastic increase in the degradation of rhodamine B (RhB) dye. This work provides a simple and efficient strategy for fabricating porous texture and realizing the tunable structure distortion of  $g\text{-C}_3\text{N}_4$  layers to adjust its electronic structure and photocatalysis.

© 2017 Elsevier B.V. All rights reserved.

## 1. Introduction

Semiconductors based photocatalysis have gained considerable interdisciplinary interest for their great potential in environmental and energetic applications such as photocatalytic degradation of pollutants and photocatalytic hydrogen generation ever since the pioneering study coauthored by Fujishima and Honda in 1972 [1,2]. Among the numerous types of photocatalysts, graphitic carbon nitride ( $g\text{-C}_3\text{N}_4$ ), since the first seminal report on  $g\text{-C}_3\text{N}_4$  photocatalysts in the  $\text{H}_2$  evolution was published in 2009 [3], has been considered as the next generation photocatalyst in the research communities, and also a step to achieving sustainability for artificial photosynthesis and environmental remediation [4]. As a metal-free polymeric photocatalyst,  $g\text{-C}_3\text{N}_4$  which is constructed from N-bridged tri-s-triazine repeating units that form two-dimensional conjugated planes packed together via van der Waals interactions, exhibits many fascinating features, such as being metal-free, appealing electronic band structure and optical properties, high chemical and thermal stability, reasonable cost, “earth-abundant” nature, flexible supermolecular networks that allow for an ease in

tuning material properties by alternating the chemical structure of backbones and so on [5,6]. However, bulk  $g\text{-C}_3\text{N}_4$  materials prepared by direct polycondensation from nitrogen-rich precursors, are still suffer some obstacles to achieve high reactivity, especially the low specific surface area, the limited active sites, and low charge carriers separation and the serious aggregation during the photocatalytic process [7,8]. Thus, many strategies have been taken to enhance the photocatalytic activity of the bulk  $g\text{-C}_3\text{N}_4$ , for instance, morphology control [9], doping with heteroatoms [10,11], constructing heterostructures [12,13], fabricating copolymers [14,15] and so on. However, developing a simple approach to modify the intrinsic structures and improve photocatalytic properties of  $g\text{-C}_3\text{N}_4$  is still desirable.

As for in-plane organization of tri-s-triazine units and the compression degree of aromatic planes,  $g\text{-C}_3\text{N}_4$  is just a typical polymer that has adjustable chemical and textural structures for photocatalysis [3]. Texture, electronic, optical, and photocatalytic properties of  $g\text{-C}_3\text{N}_4$  are strongly influenced by the condition of synthesis, such as the types of precursors [16], temperature-controlling route [17], pyrolysis temperature [18], duration employed in  $g\text{-C}_3\text{N}_4$  synthesis [19] and so on. In addition, the characteristic properties and chemical structures of  $g\text{-C}_3\text{N}_4$  are also strongly affected by the reaction atmosphere through inducing disordered structures, defects, and carbon and nitrogen vacancies [4]. Liu et al. intro-

\* Corresponding author.

E-mail address: [cwnuzhoulimei@163.com](mailto:cwnuzhoulimei@163.com) (L. Zhou).

duced nitrogen by controlling the polycondensation temperature in static air [17]. Xiong et al. reported a high-yield synthesis of g-C<sub>3</sub>N<sub>4</sub> products via heating of high vacuum-sealed melamine powder in an ampoule [20]. Tay and coworkers synthesized kinds of g-C<sub>3</sub>N<sub>4</sub> in different atmosphere (air, N<sub>2</sub>, forming gas (5%H<sub>2</sub> + 95% Ar) and pure H<sub>2</sub>), and presented defect engineered g-C<sub>3</sub>N<sub>4</sub> nanosheets produced by hydrogen treatment [21]. The hydrogenated defects in g-C<sub>3</sub>N<sub>4</sub> were also prepared by high temperature H<sub>2</sub> treatment of bulk carbon nitride [22]. An amorphous g-C<sub>3</sub>N<sub>4</sub> with a band gap of 1.90 eV was obtained by simply heating partially crystalline g-C<sub>3</sub>N<sub>4</sub> in an argon atmosphere [23]. In addition, Liang et al. synthesized holey g-C<sub>3</sub>N<sub>4</sub> nanosheets with abundant in-plane holes by thermally treating bulk g-C<sub>3</sub>N<sub>4</sub> under an NH<sub>3</sub> atmosphere [7]. Very recently, Li and coworkers prepared macroscopic foam-like holey ultrathin g-C<sub>3</sub>N<sub>4</sub> nanosheets by self-modification of polymeric melon units under an air atmosphere, and drastically improved visible-light photocatalysis [24]. These fruitful findings encourage us to think about to develop a facile method in preparing a new and high efficient photocatalytical g-C<sub>3</sub>N<sub>4</sub> material through self-modification under proper atmosphere.

As exposed, synthesizing of g-C<sub>3</sub>N<sub>4</sub> undergoes a condensation process with ammonia losses under thermal treatment of nitrogen-rich precursors such as urea, thiourea, melamine, cyanamide, dicyandiamide, and so forth [4,25]. And several researchers found g-C<sub>3</sub>N<sub>4</sub> samples by NH<sub>3</sub>-mediated polymerization process or NH<sub>3</sub>-treated had a high porosity and specific surface area, showing better photoactivity than the corresponding bulk g-C<sub>3</sub>N<sub>4</sub> [7,26,27]. So we expect designing a simple and facile way to take advantage of retainable self-producing atmosphere-NH<sub>3</sub> during pyrolysis to fabricate self-modified g-C<sub>3</sub>N<sub>4</sub>. Here, we report a facile, convenient, and most importantly simple approach to create NH<sub>3</sub> atmosphere by controlling the entrance of N<sub>2</sub> atmosphere to synthesize porous graphitic carbon nitride nanosheets with more uncondensed amino groups, as shown in Fig. 1. These formed holes endow g-C<sub>3</sub>N<sub>4</sub> nanosheets cross-plane diffusion channels that greatly speed up mass and photogenerated charge transfer. Meanwhile, these holes also provide numerous boundaries in favor of decreasing the aggregation, and more exposed active edges to promote photocatalysis. In addition, the uncondensed amino groups within the structure could generate the strong hydrogen bonding interactions between layers and thus induced the structure distortion of g-C<sub>3</sub>N<sub>4</sub> layers. As expected, compared with the bulk g-C<sub>3</sub>N<sub>4</sub>, the obtained self-modified g-C<sub>3</sub>N<sub>4</sub> show remarkably enhanced photocatalysis in the degradation process of RhB under light irradiation.

## 2. Experimental section

### 2.1. Sample preparation

The bulk g-C<sub>3</sub>N<sub>4</sub> sample was prepared by a previously reported thermal polymerization method [28]. In a typical procedure, the material was synthesized typically by heating 2.5 g of melamine in a semi-closed alumina crucible with a cover under N<sub>2</sub> gas flow to 550 °C for 4 h at a heating rate of 5 °C/min, followed by naturally cooling to room temperature. The product was collected and ground into powder and denoted as CN–N.

The self-modified g-C<sub>3</sub>N<sub>4</sub> materials were prepared mostly the same as CN–N, except stopping the entrance of N<sub>2</sub> at temperature of 500, 300, and 100 °C. The obtained samples were denoted as CN-5, CN-3, and CN-1.

### 2.2. Catalyst characterization

X-ray powder diffraction (XRD) was collected by a Rigaku Dmax/Ultima IV diffractometer with monochromatized Cu ka radiation ( $\lambda = 1.5418 \text{ \AA}$ ). Fourier transform infrared (FT-IR) spec-

troscopy was performed on a Perkin-Elmer model 2000 FTIR spectrophotometer. Scanning electron microscopy (SEM) was taken with a JEOL JSM-6510LV scanning electron microscopy. X-Ray photoelectron spectroscopy (XPS) was performed using an ESCALAB 250 Xi with a high-performance Al monochromatic source ( $h\nu = 1486.6 \text{ eV}$ , 150 W). All binding energies were referenced to the C 1s peak at 284.8 eV of surface adventitious carbon, and the elemental compositions were determined from peak area ratios after correction for the sensitivity factor for each element. And UV-vis diffuse reflectance spectra (DRS) was recorded on a Shimazu UV-3600 spectrophotometer equipped with diffuse reflectance accessories, using BaSO<sub>4</sub> as the reference sample. Brunauer-Emmett-Teller (BET) surface area was calculated from N<sub>2</sub> adsorption-desorption isotherms collected at 77 K using Quantachrome Instruments version 3.0. The photoluminescence (PL) spectra of photocatalysts were detected on a Varian Cary Eclipse spectrometer with excitation wavelength of 350 nm.

### 2.3. Photocatalytic tests

The photocatalytic activities of the prepared samples were measured by degrading RhB at ambient temperature in air with magnetic stirring. The UV-visible light was provided by a 70 W metal halide that was often used in photocatalysis conveniently [29–32]. For the degradation of RhB, 40 mg of photocatalyst was added to 80 mL of RhB aqueous solution (10 mg/L) at room temperature. Prior to irradiation, the mixture of photocatalyst and RhB suspension was firstly sonicated for 10 min and then magnetically stirred for 20 min in the dark to obtain an adsorption-desorption equilibrium. At certain time intervals, about 3 mL sample was taken out from the reaction system and centrifuged to remove the photocatalyst powders for analysis. The absorbance of the supernatant was measured using a Shimadzu UV-2550 UV-vis spectrophotometer. The relative concentration ( $C/C_0$ ) of the RhB solution was calculated at 554 nm  $C_0$  and  $C$  are the concentrations of RhB at the beginning of light irradiation and at time  $t$ , respectively.

The cyclic runs of RhB degradation was carried out to verify the stability of CN-3. After each cycle, the catalyst was collected by centrifugation, washed with distilled water, dried and then used in the next cycle without weighing. Then the photocatalytic activity was again tested.

### 2.4. Active species detection

The reactive oxidative species in the photodegradation were detected using in situ trapping experiments. The detection process was similar to the photodegradation experimental process. Three different scavengers, such as *p*-benzoquinone (BQ, •O<sub>2</sub><sup>−</sup> radicals scavenger, 1.0 mM), ammonium oxalate (AO, holes scavenger, 1.0 mM) and isopropanol (IPA, •OH radicals scavenger, 1.0 mM), were added to the RhB solution prior to illumination in three separate photodegradation systems [31,32].

## 3. Results and discussions

### 3.1. Structural characteristics

The XRD patterns of the bulk and modified g-C<sub>3</sub>N<sub>4</sub> are displayed in Fig. 2. Typically, two individual well-resolved peaks can be determined for CN–N. The strong peak at 27.2° corresponding to an inter-planar distance of approximately 0.324 nm was characterized for (002) reflection of graphitic layered materials, whereas the weak one at 13.0° ( $d = 0.685 \text{ nm}$ ) for (100) reflection can be attributed to the in-plane structural packing motif of tri-*s*-triazine units. After stopping the entrance of N<sub>2</sub>, the graphitic-like structure of g-C<sub>3</sub>N<sub>4</sub> was retained without an impurity phase [3]. However, the main

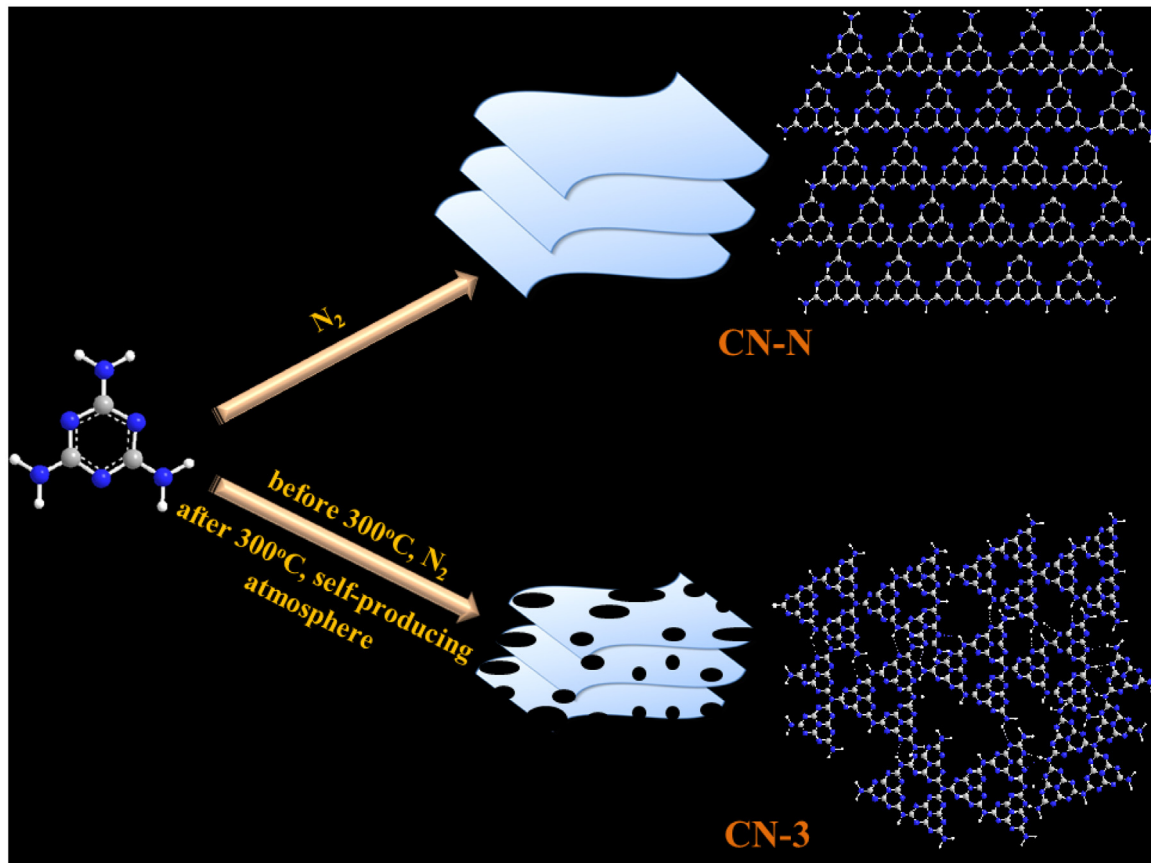


**Fig. 1.** Schematic illustration of preparing bulk g-C<sub>3</sub>N<sub>4</sub> under N<sub>2</sub> atmosphere and modified g-C<sub>3</sub>N<sub>4</sub> under self-producing atmosphere.

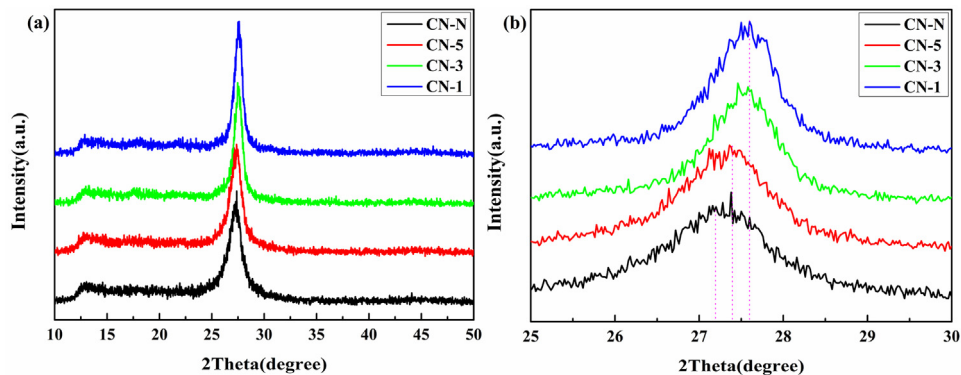


**Fig. 2.** XRD patterns of the samples treated for different methods (a) and enlarged view of (002) peak (b).

peak was slightly shifted to higher angles (Fig. 2b), CN-5 at 27.4°, both CN-3 and CN-1 at 27.6°, which reflected a reduction in the stacking distance between layer plane. Merschjann and coworkers have shown electronic transport is predominantly perpendicular to the sheets in g-C<sub>3</sub>N<sub>4</sub> [33]. So the decreased the inter-planar distance may accelerate the interlayer charge transport and thus improve the photocatalysis. The self-producing homogenous atmosphere caused layer condensation that maybe resulted in structure distortions and consequent semiconductive properties of g-C<sub>3</sub>N<sub>4</sub>. Moreover, the diffraction peak at 27.6° became narrower for CN-3, which also indicated the sample CN-3 was more uniform than CN-N.

FT-IR spectra can provide plentiful structural information concerning about different catalysts (Fig. 3). All FT-IR spectra of the as-prepared g-C<sub>3</sub>N<sub>4</sub> samples showed the similar characteristic

vibrational peaks. A series of peaks found in the range from ca. 1635–1235 cm<sup>-1</sup> attributes to the typical stretching modes of CN heterocycles. The sharp peak at ca. 810 cm<sup>-1</sup> is assigned to the bending vibration of tri-s-triazine rings, revealing that the local structure of the obtained g-C<sub>3</sub>N<sub>4</sub> is composed of tri-s-triazine units [7,16]. The sharper peak at ca. 810 cm<sup>-1</sup> and the range from ca. 1635–1235 cm<sup>-1</sup> for CN-1 and CN-3, suggests the tri-s-triazine units with more ordered in-plane structural packing motif [7]. The broad absorption band located in the range from 3650 to 3000 cm<sup>-1</sup> is originated from the stretching vibration of N–H bonds, associated with uncondensed amino groups and surface-bonded H<sub>2</sub>O molecules. The evident enhanced absorption in 3650–3000 cm<sup>-1</sup> can be considered as an indicator of CN-1, CN-3 with enlarged open-up surfaces and more uncondensed amino groups [27,34].

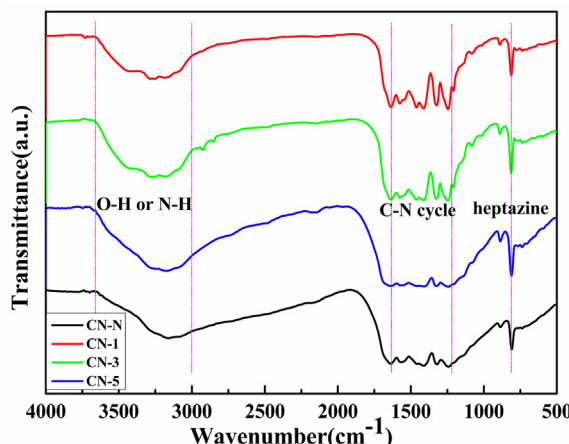


**Fig. 3.** FT-IR spectra of the samples treated for different methods.

To further evaluate the effect of self-producing atmosphere on the molecular structure of tri-s-triazine units of  $\text{g-C}_3\text{N}_4$ , the chemical composition and states were investigated by the XPS technique, and the deconvoluted high-resolution N 1s XPS spectra are shown in Fig. 4. In the XPS survey spectrum (Fig. S1, Supporting Information), only C, N and O elements were detected. The weak O 1s peak may be due to the surface absorbed  $\text{H}_2\text{O}$  or  $\text{O}_2$  [28,35]. The C 1s XPS spectra (Fig. S2, Supporting Information) displayed the main core level peak at 288.4 eV ascribed to  $\text{sp}^2$  hybridized car-

**Table 1**

Relative content of various nitrogen species on the  $\text{g-C}_3\text{N}_4$  surface obtained from N 1s XPS data(%)

Sample	$\text{C}=\text{N}-\text{C}$	$\text{N}(-\text{C})_3$	$\text{NHx}$	$\text{NHx}/\text{N}(-\text{C})_3$
CN-N	0.745	0.190	0.066	0.345
CN-5	0.767	0.157	0.076	0.481
CN-3	0.790	0.129	0.080	0.620
CN-1	0.792	0.134	0.074	0.552

bon of the tri-s-triazine rings, peak with low intensity at 286.4 eV was related to the  $\text{C}-\text{NHx}$ , peaks located at 284.9 eV and 293.4 eV originating from surface carbon contamination and  $\pi \rightarrow \pi^*$  satellite band [36–38]. The N 1s XPS of the parent  $\text{g-C}_3\text{N}_4$  can be fitted into several peaks. The main peaks at 398.9 eV, 400.2 eV and 401.4 eV were corresponded to N bonded to carbon atoms ( $\text{C}=\text{N}=\text{C}$ ) of tri-s-triazine rings, the tertiary N in the form of  $\text{N}(\text{C})_3$ , and amino functional groups ( $\text{NH}_2$  or  $\text{NH}$ ) [7,24,35], respectively. A very weak peak at 404.1 eV of N 1s was attributed to  $\pi \rightarrow \pi^*$  satellite band [36], which was very much like there is a satellite component for its C 1s signal.

The presence of tertiary N in the form of  $\text{N}(\text{C})_3$  indicated the idealized framework of carbon nitride, while the N of amino functional groups ( $\text{NH}_2$  or  $\text{NH}$ ) arose from structural defects of the carbon nitride framework [22]. Therefore, the absorptions associated with these moieties identify the defect types to some degree, as well as the uncondensed amino groups. Relative content of various nitrogen species of different  $\text{g-C}_3\text{N}_4$  are listed in Table 1. As expected, compared with CN-N, the obtained self-modified CN-5,

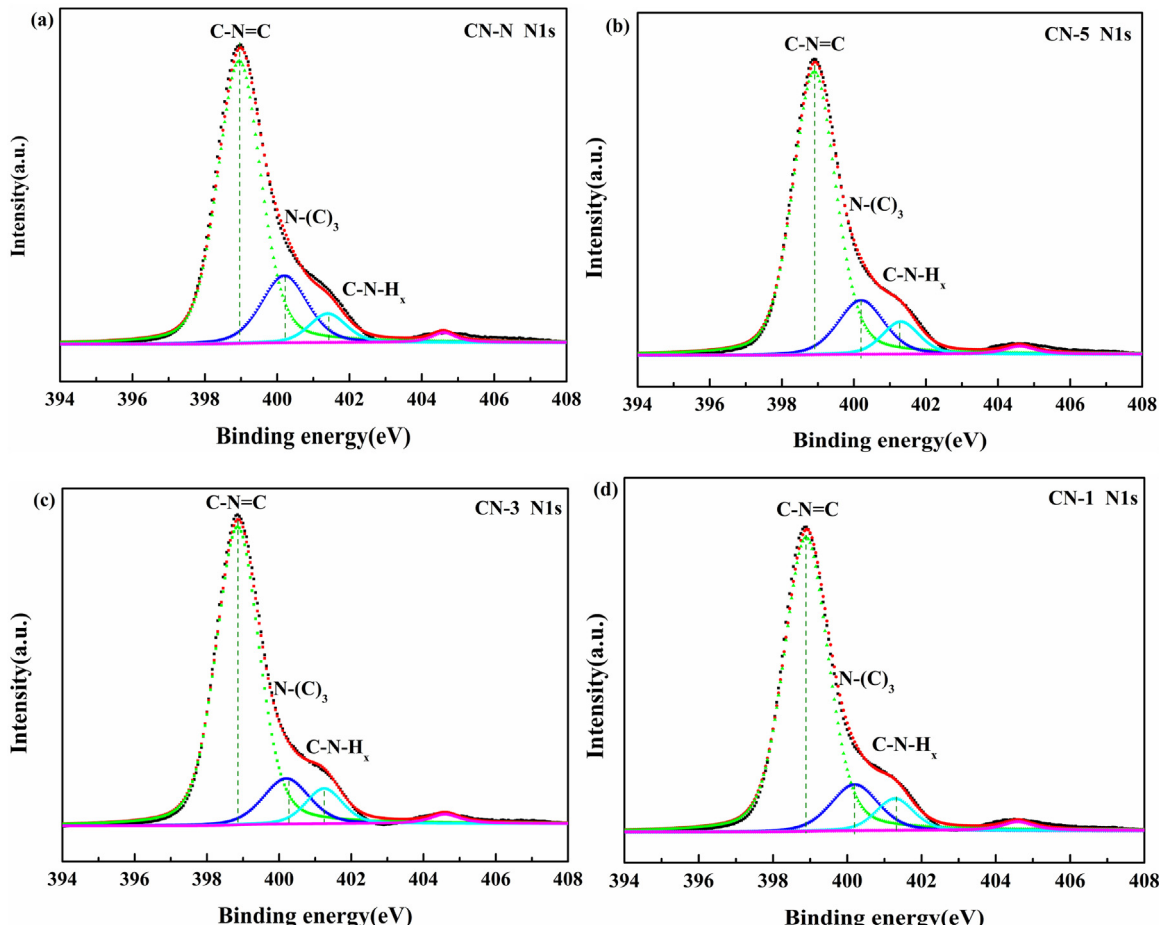


**Fig. 4.** High-resolution N1s XPS spectra of the samples treated for different methods.

CN-3 and CN-1 all show a larger value of  $\text{NH}_x/\text{N}(-\text{C})_3$ . Especially for CN-3, the value of  $\text{NH}_x/\text{N}(-\text{C})_3$  is almost 1.8 times of CN-N. These results illustrate after stopping the entrance of  $\text{N}_2$ , the pyrolysis-generated self-producing atmosphere influenced the process of thermal polymerization. A large value of  $\text{NH}_x/\text{N}(-\text{C})_3$  demonstrates a smaller polymerization degree, meanwhile a large amount of uncondensed amino groups. To explore the relative amount amino groups, we studied on the dispersion behavior of different samples in water. As shown in Fig. S3 (Supporting Information), we found self-modified CN-5, CN-3, and CN-1 were prone to disperse in water, especially CN-3. According to the report of literatures, strong hydrogen-bonding interactions between  $\text{g-C}_3\text{N}_4$  layers that arise from the presence of primary and secondary amine groups, plays a substantial role in the efficient interaction, and thus dispersibility, of exfoliated  $\text{g-C}_3\text{N}_4$  with solvents [36]. Such an outcome was attributed to a high density of uncondensed amino groups in self-modified  $\text{g-C}_3\text{N}_4$ , the presence of which was associated with incomplete condensation of the structure. The large amount of amino groups could facilitate the strong interaction between layers through the hydrogen bonding interactions and thus decreases the distance between interlayer, which was corresponding with the XRD results [28,36].

### 3.2. Textural property

The pore structures and Brunauer-Emmett-Teller (BET) surface areas of the as-prepared different samples were measured by  $\text{N}_2$  adsorption-desorption measurements at 77.4 K. As shown in Fig. 5a, all tested materials exhibit type IV isotherms with an extremely high adsorption capacity in the high relative pressure ( $P/P_0$ : from 0.8 to 1), especially CN-1 and CN-3, indicating the presence of abundant mesopores and macropores [7]. Accordingly, a sharp peak at 3.8 nm and a broad peak ranging from 12 to 180 nm are identified in the pore size distribution curve (Fig. 5b), which are, respectively, in corresponding to the diameter of the inner cavity of the  $\text{g-C}_3\text{N}_4$  nanosheets and the size of the slit-like pores formed between the  $\text{g-CN}$  nanosheets. The specific surface area and pore volume of all self-modified  $\text{g-C}_3\text{N}_4$  samples become larger compared to CN-N. The BET surface area and pore volume of CN-3 are calculated to be  $38.51 \text{ m}^2 \text{ g}^{-1}$  and  $0.44 \text{ cm}^3 \text{ g}^{-1}$ , which are about 6 times higher than those of CN-N ( $6.57 \text{ m}^2 \text{ g}^{-1}$  and  $0.076 \text{ cm}^3 \text{ g}^{-1}$ ). The higher BET surface area and larger pore volume may be caused by the effective prevention of the stacking of  $\text{g-CN}$  nanosheets by the self-producing atmosphere during the polymerization of melamine. The large surface area and pore volume could provide more reactive sites and numerous boundaries, in order to adsorb more reactants and conducive to mass transfer and charge carrier transfer during photocatalytic process [7,24,27,35].

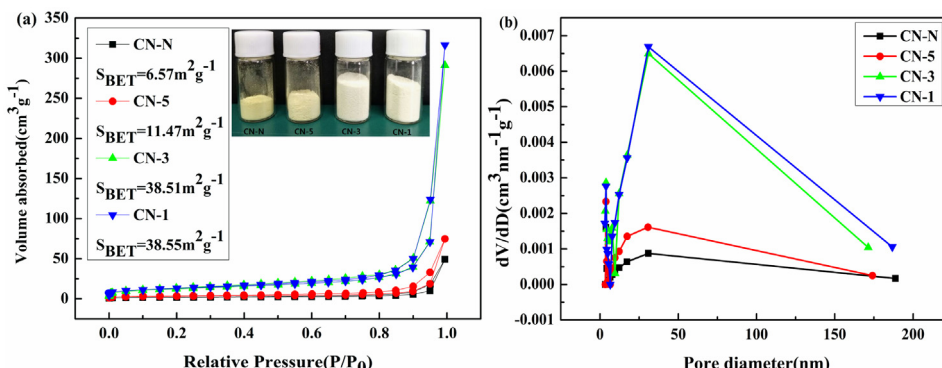


Fig. 5.  $\text{N}_2$  adsorption-desorption isotherms. Inset shows the photograph of the  $\text{g-C}_3\text{N}_4$  samples (0.4 g). (a) and BJH pore-size distribution curves (b).

### 3.3. Morphology information

The morphology and microstructure of the as-prepared samples are characterized by scanning electron microscopy (SEM). As can be seen in Fig. 6, CN-N displays disorderly stacked large and irregular clusters formed as the result of the arbitrary aggregation of small particles with sizes of around several micrometers. The bulk morphology can also be observed in the image of CN-5 sample, which indicates stopping the entrance of  $\text{N}_2$  at 500 °C could not affect too much on the processing of polycondensation. The polymeric  $\text{g-C}_3\text{N}_4$  occurred at ca. 500 °C according to reported literatures [39–41], which corresponds with our results. Far different from CN-N and CN-5, CN-1 and CN-3 exhibit more regular and homogeneous morphology. The research of Thomas et al. as well as Wang et al. demonstrate the sublimation point of melamine was ca.335 °C, while the tris-s-triazine formed via melamine rearrangements at round 390 °C [3,25]. So it's reasonable to stop  $\text{N}_2$  at 300 °C. On the one hand, the  $\text{N}_2$  could offer an inert, sole positive and atmosphere before polycondensation. On the other hand, after stopping  $\text{N}_2$ , the atmosphere constituted of melamine vapor and pyrolysis-generated  $\text{NH}_3$ . Because of the self-producing atmosphere originated from interior of reaction system, the condition of polycondensation was more homogeneous than common thermal condensation, so we obtained regular and homogeneous morphology. Meanwhile, self-producing ammonia resulted large amount holes and broke the equilibrium of polycondensation to decrease the degree. The sample of CN-1 has a similar state as CN-3. Because stopping  $\text{N}_2$  at 100 °C, so the atmosphere pressure decreased and became disorder ahead of polycondensation. At this condition, the self-producing atmosphere and melamine vapor could easily drop away, and resulted smaller particles. As far as we know, this is the first research focusing on the influence of the self-producing atmosphere on  $\text{g-C}_3\text{N}_4$  synthesis.

### 3.4. Optical properties

It is expected that these unique porous nanosheets containing more uncondensed amino groups would have a large effect on the optical properties and electronic band structure of  $\text{g-C}_3\text{N}_4$ . To identify the electronic structure and photoelectric property of different materials, UV-vis diffuse reflectance spectroscopy (DRS) (Fig. 7a) and photoluminescence (PL) (Fig. 7b) spectra were used. UV-vis DRS spectra indicates that the absorption edge of self-modified  $\text{g-C}_3\text{N}_4$  samples display a remarkable blue shift (from ~460 to 430 nm) in comparison with the CN-N. The results are consistent with pale yellow color as well as low degree of polycondensation. Accordingly, the derived electronic band gaps from the Tauc plots (in which  $(F(R)hv)^{1/2}$  is plotted versus the photon energy ( $h\nu$ ),  $F(R)$

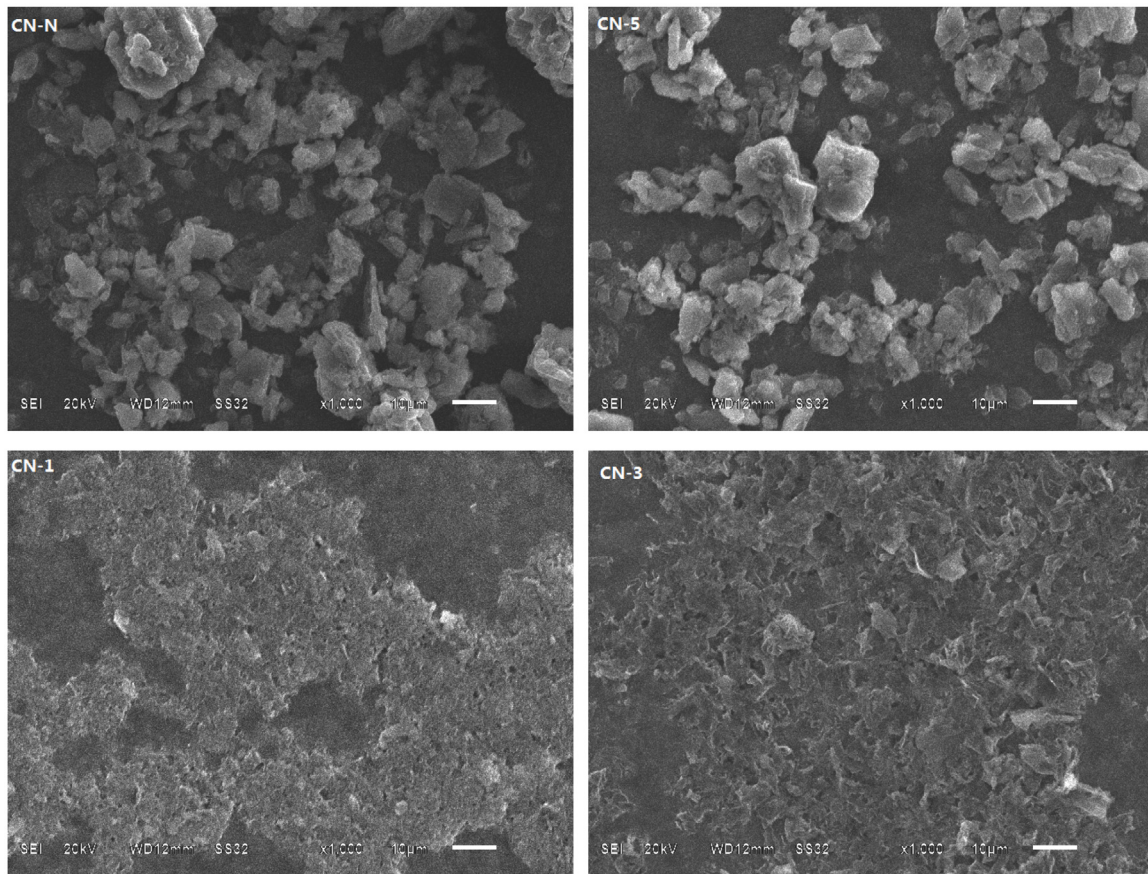


**Fig. 6.** SEM patterns of  $\text{g-C}_3\text{N}_4$  samples treated for different methods.

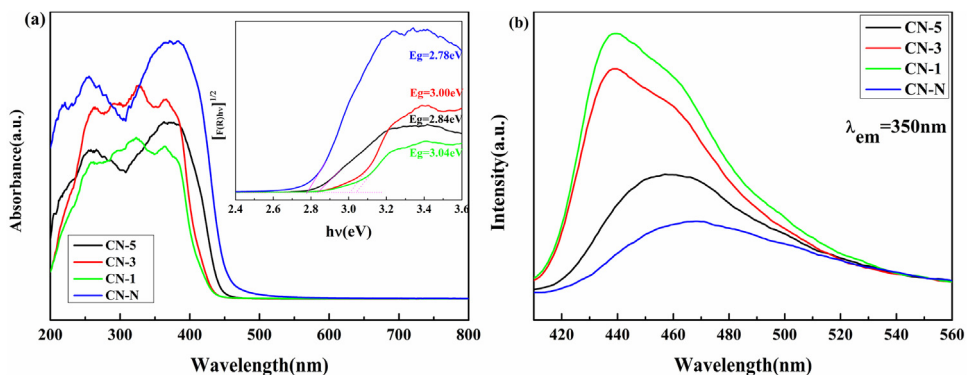


**Fig. 7.** (a) UV-vis diffuse reflectance of spectra and (b) Steady-state PL spectra.

is the diffuse absorption coefficient,  $h$  is the Planck constant, and  $v$  is the light frequency) are 3.04 eV for CN-1, 3.00 eV for CN-3, 2.84 eV for CN-5, 2.78 eV for CN-N, respectively (inset in Fig. 7a). The bandgaps of CN-1, CN-3 and CN-5 are widened by 0.26 eV, 0.22 eV, 0.06 eV compared to CN-N, respectively. The results are further confirmed by the blue-shifts of their fluorescence emission peaks in Fig. 7b, which should be attributed to the quantum confinement effect [7,24,41]. In addition, the absorbance curves of CN-1 and CN-3 appear a new peak at ca. 325 nm compared to CN-N and CN-5, which demonstrate the self-modified  $\text{g-C}_3\text{N}_4$  can greatly improve the ability of  $\text{g-C}_3\text{N}_4$  to harvest light.

PL emission spectra originating from the recombination of free charge carriers are important to reveal the separation, migration and recombination of photogenerated charge carriers. According to the report of literature, the photoluminescence spectrum sen-

sitively depends on the degree of condensation and the packing between the layers of different  $\text{g-C}_3\text{N}_4$  materials [25], and the PL intensity of the  $\text{g-C}_3\text{N}_4$  decreases when the emission peaks redshift, which is due to the decreased number of emission centers, because of the enhanced condensation degree of the  $\text{g-C}_3\text{N}_4$  and the enhanced disorder of the microstructure for CN-N [42–44]. As shown in Fig. 7b, all excitation spectra were monitored at room temperature with an excitation wavelength of 350 nm, and match well with UV-vis diffuse reflectance spectra. The blue-shifts wavelength of fluorescence emission peak illustrates smaller degree polycondensation of self-modified  $\text{g-C}_3\text{N}_4$  comparing to CN-N. In addition, CN-1, CN-3, CN-5 show higher fluorescence intensity than CN-N. This results further confirm smaller degree opolycondensation of self-modified  $\text{g-C}_3\text{N}_4$  materials, and illustrate the uncondensed amino groups may play role of emission centers. Note

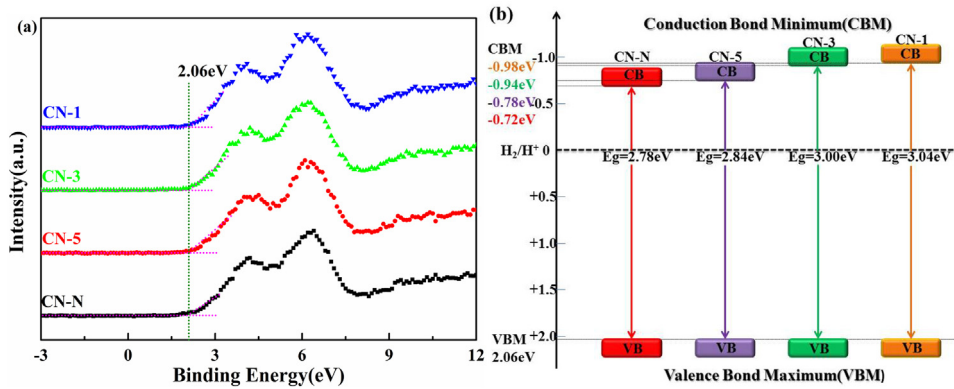


Fig. 8. (a) XPS valence band and (b) illustration of the band gap structures.

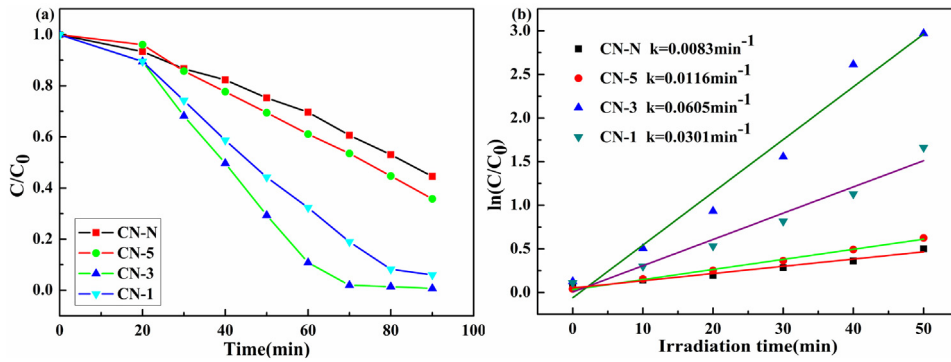


Fig. 9. (a) Photocatalytic degradation of RhB and (b) First-order kinetic plots for degradation.

the CN–N has a low PL emission peak, which is associated with its inconsistent structure, as evidenced by XRD [43].

To further research the influence of self-producing atmosphere on positions of the conduction band (CB) and valence band (VB) of samples, the valence band X-ray photoelectron spectroscopy (VB XPS) was tested. From Fig. 8a, it can be known that all the samples have the same VB of ~2.06 eV. Combined with the UV-vis DRS result, we found that the CB of all self-modified g-C<sub>3</sub>N<sub>4</sub> samples were upshifted, which indicates stronger redox abilities of modified g-C<sub>3</sub>N<sub>4</sub> samples [27].

### 3.5. Photocatalytic performance

The photocatalytic activities of all the samples were evaluated by the evolution of RhB degradation as a function of time under UV-visible light illumination. It is important to note that no degradation of RhB occurs under illumination without photocatalyst [30,31]. As shown in Fig. 9a, after 50 min of irradiation, ca. 40% of RhB is degraded in the presence of CN–N, while the self-modified g-C<sub>3</sub>N<sub>4</sub> samples all show superior efficiency than CN–N. Especially for CN-3, approximately 98% of RhB is decomposed in 50 min of irradiation. The photocatalytic data were subsequently fitted by a pseudo-first-order model to study reaction kinetics of the RhB degradation and the corresponding apparent reaction constants (k) are shown in Fig. 9b. It is obvious that sample CN-3 owns the best catalytic degradation ability, which is 7.3 times higher than the CN–N sample.

The stability of a photocatalyst is also very important from the point of its practical application. The CN-3 sample was tested through six consecutive trials of photocatalytic degradation of RhB (Fig. 10a). With the reaction time prolonged, RhB rapidly

degraded in the presence of CN-3 with no obvious deactivation, demonstrating reusability and stability of the CN-3. Therefore, CN-3 can be regarded as a stable high-performance photocatalyst for photodegrading organic pollutants, possessing great prospects in environmental protection. In addition, the catalyst CN-3 after the six photodegradation runs was further measured by SEM, XRD, FTIR, XPS, and UV-vis diffuse reflectance. These characterization results of the CN-3 before and after the repeated reactions were almost the same, indicated that the CN-3 was stable (Fig. S4–8, Supporting Information). But the mass loss of catalyst was nonnegligible. The mass loss rate reached up to 61.2% (Fig. S9, Supporting Information). So the loss of catalyst CN-3 in recycling experiment may be the major factor affected the photocatalyst reactivation.

### 3.6. Mechanism for the photocatalysis

It has been known when the photocatalyst is irradiated by light, the electrons and holes can be produced in CB and VB. It is well known the holes have the ability of oxidation, and while the electrons have the ability of reduction. From Fig. 8b, one can see that the conduction band edge potential of CN-3 (-0.94 eV vs NHE) is more negative than the standard redox potential O<sub>2</sub>/•O<sub>2</sub><sup>-</sup> (-0.046 V vs NHE) to reduce the molecular oxygen to yield •O<sub>2</sub><sup>-</sup> [45]. However, the VB potential of CN-3 (+2.06 eV vs NHE) is nearly the same as the standard redox potential of OH<sup>-</sup>/•OH (+1.99 V vs NHE) [45]. Hence, we may infer the photoinduced h<sup>+</sup> cannot efficiently oxidize OH<sup>-</sup> to generate •OH radicals (Fig. 11).

To confirm our hypothesis and probe the main active species involved in the degradation process, the trapping experiments of the composites were conducted. In this study, ammonium oxalate (AO), p-benzoquinone (BQ), and isopropyl alcohol (IPA)

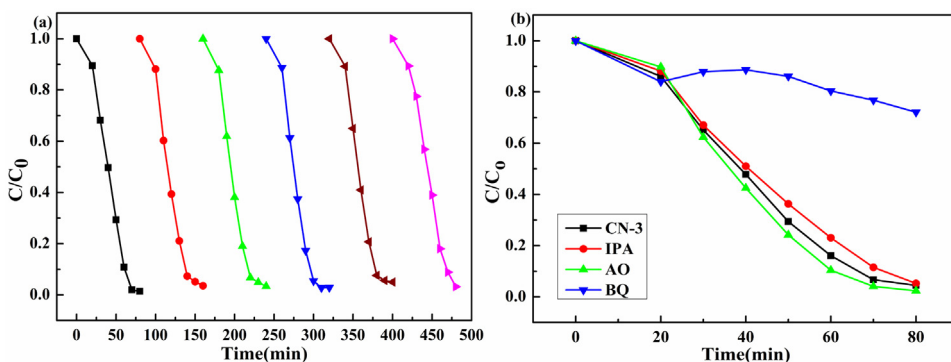


**Fig. 10.** (a) Reusability of sample CN-3 and (b) Photocatalytic activities of CN-3 for the degradation of RhB in the presence of different scavengers.

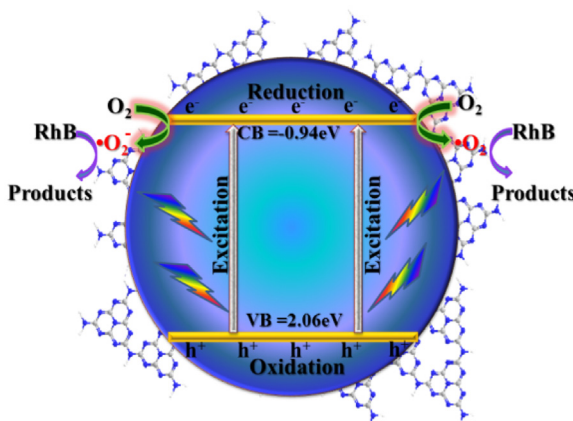


**Fig. 11.** Schematic illustration for the photocatalytic degradation of RhB dye over CN-3.

were employed as the scavengers for photo-generated holes ( $h^+$ ), superoxide radical ( $\cdot O_2^-$ ) and hydroxyl radical ( $\cdot OH$ ), respectively [30,31]. From Fig. 10b, as expected the photocatalytic activity of CN-3 is greatly suppressed by the addition of BQ, indicating that  $\cdot O_2^-$  is the main active species in the photocatalytic reaction. Conversely, no obvious decrease in the photocatalytic activity are observed by introduction of IPA or AO, which demonstrate the  $\cdot OH$  and  $h^+$  radicals are not the dominating active species in the photocatalytic reaction.

#### 4. Conclusions

In conclusion, porous g-C<sub>3</sub>N<sub>4</sub> with more uncondensed amino groups was prepared by heating melamine under self-producing atmosphere for the first time. The self-producing atmosphere can create a well-distributed condition and induce the process of condensation, thus significantly improved the intrinsic optical properties and photocatalytic activity of g-C<sub>3</sub>N<sub>4</sub>. The drastic enhancement of photocatalytic activity for CN-3 is attributed to the following factors. First of all, the uncondensed amino groups within the structure efficiently induce the distortion of planar structure and decreases the distance of interlayer, thus improve charge carrier transporting in the material. In addition, porous structure of g-C<sub>3</sub>N<sub>4</sub> nanosheets can provide a large specific surface area, more exposed new edges, and catalytic active sites, and also the sufficient porosity of samples facilitates the rapid diffusion of mass, photogenerated carriers. Third, the high dispersity of CN-3 in water resulting from the uncondensed amino groups may greatly improve contact between g-C<sub>3</sub>N<sub>4</sub> and reactant molecules. Overall, this work provides a new simple and effective strategy for improving the intrinsic electronic structures and photocatalytic performance of

g-C<sub>3</sub>N<sub>4</sub>. The excellent photocatalytic performance and stability indicate that the material may be used as an efficient and sustainable photocatalyst in aqueous solution.

#### Acknowledgement

The authors are grateful for financial support from the Natural Science Foundation of China (21303139).

#### Appendix A. Supplementary data

Supplementary data associated with this article can be found, in the online version, at <http://dx.doi.org/10.1016/j.apcatb.2017.05.084>.

#### References

- [1] A. Fujishima, K. Honda, *Nature* 238 (1972) 37–38.
- [2] S. Cao, J. Low, J. Yu, M. Jaroniec, *Adv. Mater.* 27 (2015) 2150–2176.
- [3] X. Wang, K. Maeda, A. Thomas, K. Takanabe, G. Xin, J.M. Carlsson, K. Domen, M. Antonietti, *Nature* 8 (2009) 76–80.
- [4] W.J. Ong, L.L. Tan, Y.H. Ng, S.T. Yong, S.P. Chai, *Chem. Rev.* 116 (2016) 7159–7329.
- [5] B.V. Lotsch, M. Doblinger, J. Sehnert, L. Seyfarth, J. Senker, O. Oeckler, W. Schnick, *Chemistry* 13 (2007) 4969–4980.
- [6] Y. Wang, X. Wang, M. Antonietti, *Angew. Chem.* 51 (2012) 68–89.
- [7] Q. Liang, Z. Li, Z.-H. Huang, F. Kang, Q.-H. Yang, *Adv. Funct. Mater.* 25 (2015) 6885–6892.
- [8] J. Liu, H. Wang, M. Antonietti, *Chem. Soc. Rev.* 45 (2016) 2308–2326.
- [9] Z. Tong, D. Yang, Y. Sun, Y. Nan, Z. Jiang, *Small* 12 (2016) 4093–4101.
- [10] J. Xue, S. Ma, Y. Zhou, Z. Zhang, M. He, *ACS Appl. Mat. Interfaces* 7 (2015) 9630–9637.
- [11] G. Zhang, M. Zhang, X. Ye, X. Qiu, S. Lin, X. Wang, *Adv. Mater.* 26 (2014) 805–809.
- [12] J.C. Wang, H.C. Yao, Z.Y. Fan, L. Zhang, J.S. Wang, S.Q. Zang, Z.J. Li, *ACS Appl. Mat. Interfaces* 8 (2016) 3765–3775.
- [13] X. Zhang, B. Peng, S. Zhang, T. Peng, *ACS Sustainable Chem. Eng.* 3 (2015) 1501–1509.
- [14] X. Fan, L. Zhang, R. Cheng, M. Wang, M. Li, Y. Zhou, J. Shi, *ACS Catal.* 5 (2015) 5008–5015.
- [15] J. Zhang, X. Chen, K. Takanabe, K. Maeda, K. Domen, J.D. Epping, X. Fu, M. Antonietti, X. Wang, *Angew. Chem. Int. Ed.* 49 (2010) 441–444.
- [16] H. Lan, L. Li, X. An, F. Liu, C. Chen, H. Liu, J. Qu, *Appl. Catal. B: Environ.* 204 (2017) 49–57.
- [17] P. Niu, G. Liu, H.-M. Cheng, *J. Phys. Chem. C* 116 (2012) 11013–11018.
- [18] H. Zhang, A. Yu, *J. Phys. Chem. C* 118 (2014) 11628–11635.
- [19] F. Dong, Z. Wang, Y. Sun, W.K. Ho, H. Zhang, *J. Colloid Interface Sci.* 401 (2013) 70–79.
- [20] Y. Yuan, L. Zhang, J. Xing, M.I. Utama, X. Lu, K. Du, Y. Li, X. Hu, S. Wang, A. Genc, R. Dunin-Borkowski, J. Arbiol, Q. Xiong, *Nanoscale* 7 (2015) 12343–12350.
- [21] Q. Tay, P. Kanhere, C.F. Ng, S. Chen, S. Chakraborty, A.C.H. Huan, T.C. Sum, R. Ahuja, Z. Chen, *Chem. Mater.* 27 (2015) 4930–4933.
- [22] X. Li, G. Hartley, A.J. Ward, P.A. Young, A.F. Masters, T. Maschmeyer, *J. Phys. Chem. C* 119 (2015) 14938–14946.
- [23] Y. Kang, Y. Yang, L.C. Yin, X. Kang, G. Liu, H.M. Cheng, *Adv. Mater.* 27 (2015) 4572–4577.
- [24] Y. Li, R. Jin, Y. Xing, J. Li, S. Song, X. Liu, M. Li, R. Jin, *Adv. Eng. Mater.* 6 (2016) 1601273.
- [25] A. Thomas, A. Fischer, F. Goettmann, M. Antonietti, J.-O. Müller, R. Schlägl, J.M. Carlsson, *J. Mater. Chem.* 18 (2008) 4893–4908.

[26] P. Yang, J. Zhao, W. Qiao, L. Li, Z. Zhu, *Nanoscale* 7 (2015) 18887–18890.

[27] Y. Cui, G. Zhang, Z. Lin, X. Wang, *Appl. Catal. B: Environ.* 181 (2016) 413–419.

[28] W. Ho, Z. Zhang, M. Xu, X. Zhang, X. Wang, Y. Huang, *Appl. Catal. B: Environ.* 179 (2015) 106–112.

[29] L. Ming, H. Yue, L. Xu, F. Chen, *J. Mater. Chem. A* 2 (2014) 19145–19149.

[30] J. Shu, Z. Wang, G. Xia, Y. Zheng, L. Yang, W. Zhang, *J. Chem Eng* 252 (2014) 374–381.

[31] N. Huang, J. Shu, Z. Wang, M. Chen, C. Ren, W. Zhang, *J. Alloys Compd.* 648 (2015) 919–929.

[32] H.-B. Fang, Y. Luo, Y.-Z. Zheng, W. Ma, X. Tao, *Ind. Eng. Chem. Res.* 55 (2016) 4506–4514.

[33] C. Merschjann, S. Tschierlei, T. Tyborski, K. Kailasam, S. Orthmann, D. Hollmann, T. Schedel-Niedrig, A. Thomas, S. Lochbrunner, *Adv. Mater.* 27 (2015) 7993–7999.

[34] Q. Han, B. Wang, J. Gao, Z. Cheng, Y. Zhao, Z. Zhang, L. Qu, *ACS nano* 10 (2016) 2745–2751.

[35] Q. Liang, Z. Li, X. Yu, Z.H. Huang, F. Kang, Q.H. Yang, *Adv. Mater.* 27 (2015) 4634–4639.

[36] M. Ayan-Varela, S. Villar-Rodil, J.I. Paredes, J.M. Munuera, A. Pagan, A.A. Lozano-Perez, J.L. Cenís, A. Martínez-Alonso, J.M. Tascon, *ACS Appl. Mat. Interfaces* 7 (2015) 24032–24045.

[37] W. Xing, G. Chen, C. Li, J. Sun, Z. Han, Y. Zhou, Y. Hu, Q. Meng, *ChemCatChem* 8 (2016) 2838–2845.

[38] X. She, L. Liu, H. Ji, Z. Mo, Y. Li, L. Huang, D. Du, H. Xu, H. Li, *Appl. Catal. B: Environ.* 187 (2016) 144–153.

[39] Z. Mo, X. She, Y. Li, L. Liu, L. Huang, Z. Chen, Q. Zhang, H. Xu, H. Li, *RSC Adv.* 5 (2015) 101552–101562.

[40] J. Liu, T. Zhang, Z. Wang, G. Dawson, W. Chen, *J. Mater. Chem.* 21 (2011) 14398–14401.

[41] G. Zhang, J. Zhang, M. Zhang, X. Wang, *J. Mater. Chem.* 22 (2012) 8083–8091.

[42] Y. Zhao, Z. Liu, W. Chu, L. Song, Z. Zhang, D. Yu, Y. Tian, S. Xie, L. Sun, *Adv. Mater.* 20 (2008) 1777–1781.

[43] F. Dong, Z. Zhao, T. Xiong, Z. Ni, W. Zhang, Y. Sun, W.K. Ho, *ACS Appl. Mat. Interfaces* 5 (2013) 11392–11401.

[44] M. Shalom, S. Inal, C. Fettkenhauer, D. Neher, M. Antonietti, *J. Am. Chem. Soc.* 135 (2013) 7118–7121.

[45] Y. Yang, Y. Guo, F. Liu, X. Yuan, Y. Guo, S. Zhang, W. Guo, M. Huo, *Appl. Catal. B: Environ.* 142–143 (2013) 828–837.